Transient liquid phase sintering of high density Fe_3Al using Fe and Fe_2Al_5 / $FeAl_2$ powders Part 1: Experimentation and results

N. K. Xydas, B. L. Gabbitas, X. X. Xu and L. A. Salam

High density Fe_3Al was produced through transient liquid phase sintering, using rapid heating rates of greater than 150 K min^{-1} and a mixture of prealloyed and elemental powders. Prealloyed $Fe_2Al_5/FeAl_2$ (50Fe/50Al, wt-%) powder was added to elemental iron powder in a ratio appropriate for producing an overall Fe_3Al (13·87 wt-%) ratio. The heating rate, sintering time, sintering temperature, green density and powder particle size were controlled during the study.

Heating rate, sintering time and powder particle size had the most significant influence upon the sintered density of the compacts. The highest sintered density of 6·12 Mg m^{-3} (92% of the theoretical density for Fe_3Al) was achieved after 15 minutes of sintering at 1350°C, using a 250 K min^{-1} heating rate, 1–6 μm Fe powders and 5·66 μm alloy powders.

SEM microscopy suggests that agglomerated $Fe_2Al_5/FeAl_2$ particles, which form a liquid during sintering, are responsible for a significant portion of the remaining porosity in high sintered density compacts, creating stable pores, larger than 100 μm diameter, after melting.

High density was achieved by minimising the Kirkendall porosity formed during heating by unbalanced diffusion and solubility between the iron and $Fe_2Al_5/FeAl_2$ components. The lower diffusion rate of aluminium in the prealloyed powder into the iron compared with elemental aluminium in iron, coupled with a fast heating rate, is expected to permit minimal iron–aluminium interdiffusion during heating so that when a liquid forms the aluminium dissolves in the iron to promote solidification at a lower aluminium content. This leads to a further reduction in porosity.

PM/1021

Dr Xydas (nick_xydas@xtra.co.nz) was formerly in the Faculty of Engineering Science and Technology, South Bank University, London, UK. Dr Gabbitas (briang@waikato.ac.nz) is in the Department of Materials and Process Engineering, University of Waikato, Private Bag 3105, Hamilton, New Zealand. Dr Xu and Dr Salam are in the Faculty of Engineering Science and Technology, South Bank University, London, SE1 0AA, UK. Manuscript received 13 August 2002; accepted 5 November 2002.

INTRODUCTION

This paper describes experimental work carried out to identify the influential parameters controlling the density of sintered iron–aluminium intermetallics, to produce Fe_3Al, without the application of external pressure.

Iron aluminides, particularly Fe_3Al, possess good high temperature strength, excellent oxidation and sulphidation resistance and good wear and cavitation resistance.[1,2] Because of this, these alloys have been suggested as possible substitutes for 300 and 400 series stainless steels and some of the nickel based superalloys.[3] This is because the low raw material cost of iron–aluminium intermetallics and the low density of some of the iron–aluminium alloys offer a superior strength to weight ratio compared with stainless steels. However, a lack of interest in this system for structural applications can be largely attributed to poor room temperature ductility and poor high temperature strength using current processing methods. More recently[4–6] research has identified the mechanisms leading to embrittlement and more ductile alloys can now be produced. The intermetallics FeAl and Fe_3Al are not expected to be brittle since they possess strong grain boundaries and exhibit {110}·111· slip. High temperature strength is largely dictated by the stability of the DO_3 structure of Fe_3Al relative to the B_2 of FeAl. Strength improvements were reported,[7,8] as a result of work carried out to increase the DO_3–B_2 transition temperature.

Iron–aluminides containing more than 16 at.-% aluminium are susceptible to hydrogen embrittlement when strained in the presence of water vapour. Methods for overcoming poor ductility have received a lot of attention,[4] with investigations directed towards the effects of oxygen and alloying additions such as chromium. Recent advances relating to a better understanding and control of environmental embrittlement have strengthened interest in iron–aluminides and research into feasible low cost production methods. The intermetallics FeAl and Fe_3Al are commonly cast, an economical method for production, but one which can lead to absorption of large amounts of hydrogen deriving from moisture in the process. This promotes hydrogen embrittlement and causes porosity in the alloy. Although vacuum processing can be used, this increases production costs.

Sintering of iron–aluminides is attractive because of the production cost reductions and the microstructural control that is afforded by powder metallurgy production routes. Sintering in the presence of a liquid phase can facilitate rapid sintering of high density components exhibiting a variety of microstructures.[10] The application of the component usually determines the processing parameters employed, although the majority of applications require the optimum mechanical properties usually associated with minimum porosity. Exceptions from the rule include refractory components, composites and deliberately porous components, produced by careful parameter control. Poor dimensional control can cause problems during liquid phase sintering and even a loss of compact shape where excessive liquid is present.

Progress towards sintering high density Fe_3Al has been slow, due to the mismatch in diffusion and solubility rates of elemental iron and aluminium. Iron has a low solubility and diffusion rate in aluminium whereas aluminium has a much higher solubility and diffusion rate in iron. Studies[11,12] carried out on the titanium–aluminium and zinc–aluminium systems have shown that mismatched diffusion and solubility rates promote swelling during sintering and consequently

 DOI 10.1179/003258903225010497

a high degree of porosity. In the iron–aluminium system, Kirkendall porosity forms at aluminium particle sites after diffusion of aluminium into iron, resulting in swelling, a lowering of the average density and the formation of various stable iron–aluminium compounds around pores, which prevent any further densification. Various techniques for achieving high densities in iron aluminides have been reported in the literature. Reactive sintering has been successfully applied to nickel aluminide, Ni_3Al,[13] where the reaction energy between the elemental components allows the reaction to initiate at low temperatures and the characteristics of the system allow a high density to be achieved. A similar technique has been attempted using the iron–aluminium system,[14] but swelling inhibited the achievement of a high density. It has been reported[15,16] that additions of a few per cent of nickel inhibit swelling and higher densities are achievable, but nickel is expensive. Also reference to the Ni–Al–Fe ternary phase diagram shows that since the Fe_3Al phase is not present at up to 15% nickel concentations, there are doubts about the usefulness of these ternary compositions in structural and high temperature applications.

The most promising route to a high sintered density is through the use of suitable prealloyed powders. In particular, the addition of a prealloyed powder as a transient liquid forming constituent looks attractive. Such a technique has been investigated, with some success, using the iron–titanium system[17–20] where it was suggested that heating rate and powder particle size are important in controlling sintered density. Such an approach, using the iron–aluminium system, has so far only received limited attention.[21]

This paper describes the results of experimental work, to investigate the pressureless sintering of iron and pre-alloyed iron–aluminium powders, designed to overcome the iron–aluminide densification problems.

EXPERIMENTAL PROCEDURE

Iron powder (Fe) and prealloyed $Fe_2Al_5/FeAl_2$ (50/50 wt-%) powder, mixed in the ratio of Fe_3Al, was used in these experiments. The iron powder size was 1–6 μm and more than 98% pure, obtained from Goodfellow, Cambridge, UK. The 50–50wt-% iron–aluminium alloy powder was obtained from Essex Metallurgical, Canvey Island, Essex, UK, with a 45 μm powder particle size and 99·7% pure. X-ray diffraction was conducted on the alloy powder to verify the presence of the two crystal structures Fe_2Al_5 and $FeAl_2$ and the absence of significant quantities of other iron–aluminium phases. The alloy powder was then ball milled in a Fritsch planetary ball mill model (PM5/2), in sealed vials containing argon greater than 99·8% purity. Ball milling for 10 minutes and 25 minutes produced two fine sized powders for which the size distribution was verified using a Coulter laser particle size analyser LS-230. The particle size distributions after 10 and 25 minutes of milling are shown in Fig. 1*a* and *b* for three separate measurements. The mean average particle size after 10 minutes of milling was found to be 15·58 μm and after 25 minutes it was 5·67 μm. This was subsequently verified by SEM microscopy.

The powders were mixed in a low density polyethylene (LDPE) bottle for 30 minutes, then pressed into cylindrical discs with a diameter of 15 mm and heights of 2·55 mm or 2·8 mm under two pressures of 56 MPa and 168 MPa, which gave samples with green densities of 61% and 67% of theoretical density respectively. Die wall lubricants and additives were not used. A higher green density was avoided to facilitate liquid flow during sintering. Sintering was carried out in an argon atmosphere of greater than 99·8% purity.

Four heating rates, 20, 150, 250 and 400 K min^{-1} were used to sinter the powders. The 20 K min^{-1} heating rate was achieved in a horizontal tube electrical resistance furnace, while the faster heating rates were obtained using a radio frequency (RF) induction furnace.

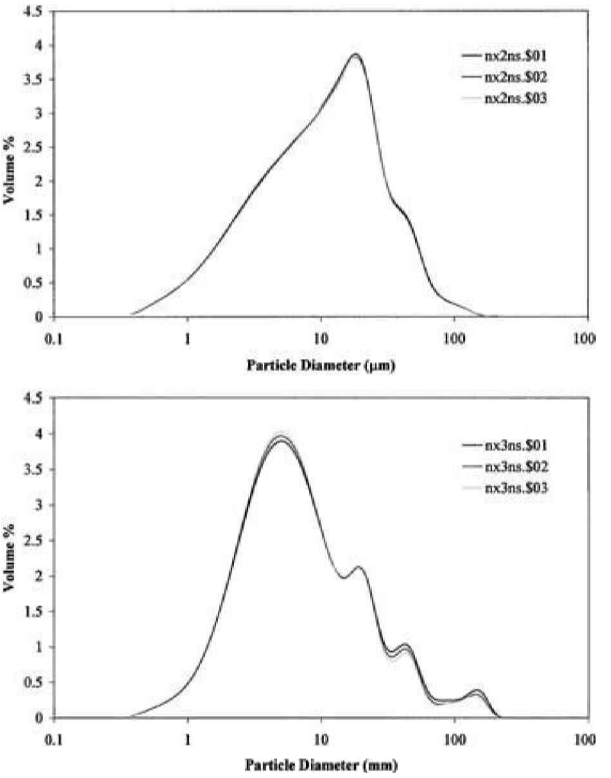

a a 10 min; *b* 25 min

1 Particle size distribution of $Fe_2Al_5/FeAl_2$ powder after milling for different times in argon

Sintered sample densities were measured using Archimedes' principle as specified in BS 5600 part 3 section 3.2. The microstructures of sintered and quenched samples at different temperatures were examined using scanning electron microscopy (SEM) and optical microscopy.

RESULTS AND DISCUSSION

In order to optimise the sintering process, an experimental programme was devised to investigate the effect of powder size, compaction pressure, heating rate, sintering temperature and holding time at the sintering temperature on the sintered density. Many experiments were performed and a selection of these results is compared in Table 1, along with the important variables. Green and sintered densities are shown as a percentage of the theoretical density of Fe_3Al, which is 6·65 g cm^{-3}. The densification parameter φ is used to compare density changes in samples with different green densities and is defined in equation (1) as

$$\varphi = \frac{\rho_s - \rho_g}{1 - \rho_g} \quad \ldots\ldots\ldots\ldots\ldots\ldots \quad (1)$$

where ρ_s is fractional sintered density and ρ_g is fractional green density. The highest density achieved was 92% with a densification of 82·2%, after 15 minutes at 1350°C, using a heating rate of 250 K min^{-1} and starting from a green density of 61%.

Each sample produced was analysed using energy dispersive X-ray (EDX), electron probe microanalysis techniques (EPMA) and X-ray diffraction (XRD) techniques and found to contain homogenous Fe_3Al with small inclusions of impurity but no other Fe–Al phase.[9]

Heating rate effects on density

Figure 2 illustrates the effect of heating rates from 20 K min^{-1} to 400 K min^{-1} on sintered density, using sintering times of up to 15 minutes at 1300°C. The 20 K min^{-1} heating

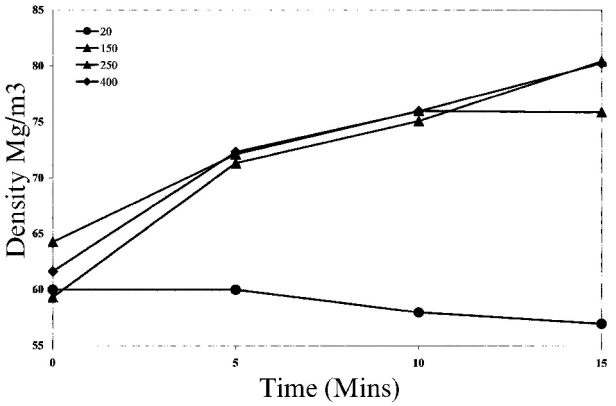

2 Comparison of 20, 150, 250 and 400 K min^{-1} heating rates for Fe_3Al compacts sintered at 1300°C for 0, 5, 10 and 15 min

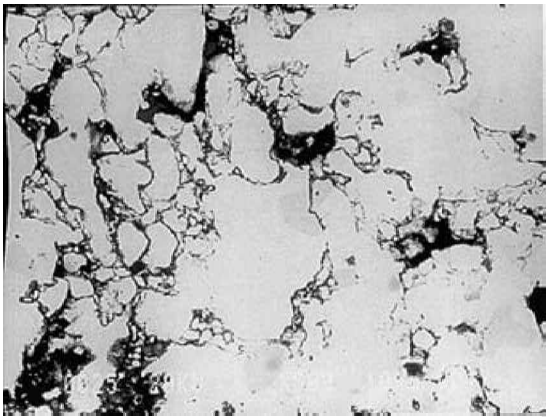

3 SEM micrograph of compact heated at 20 K min^{-1} and sintered for 15 min (×500)

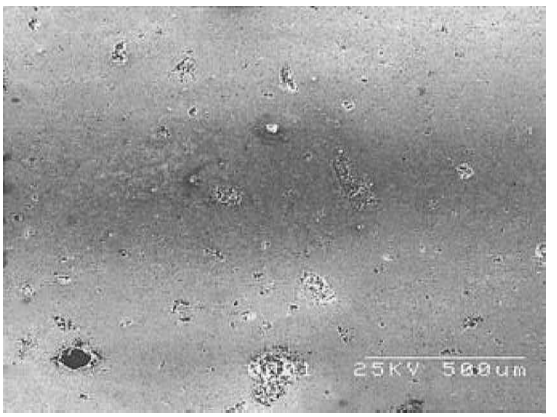

4 SEM micrograph of sample heated at 150 K min^{-1} and sintered for 15 min

rate caused continuous expansion, so that after sintering for 15 minutes the sintered density was 55%, or 6% less than the green density. Samples heated at 150, 250 or 400 K min^{-1} show a continuous increase in density with time, the maximum in each case occurring after 15 minutes. The results showed that heating rates greater than 150 K min^{-1} produced no greater improvement in sintered density.

This difference in behaviour between the 20 K min^{-1} heating rate and the 150 K min^{-1} and higher rates suggests that a different sintering mechanism is present in each case. It is hypothesised that at slower heating rates the diffusion between the Fe_2Al_5/Fe_3Al_2 and the Fe powders whilst in solid state (i.e below the 1162°C melting point of the alloy) is high enough that once the 1162°C temperature is reached, the $Fe_2Al_5/FeAl_2$ phases are no longer present. This results in a lack of liquid formation and a lack of densification associated with rearrangement from liquid presence, which appear to be present with the higher heating rates.[9]

At 150 K min[1] heating rates or greater, there were small variations in density from changes in heating rates after a given sintering time and temperature. These variations were small enough to fall within the expected experimental error, inferring no significant advantage to using a heating rate greater than 150 K min^{-1}. The only exception to this was in samples heated at 150 K min^{-1} to 1300°C and sintered for 15 minutes. The density of these sintered samples was consistently the same or lower than the values found after 10 minutes of sintering inferring the presence of an expansion mechanism at sintering times greater than 10 minutes under these conditions. It is suggested that this may be due to Ostwald ripening, a process by which large grains grow at the expense of smaller, allowing porosity volume to increase. This would be expected if sintering was to continue after maximum sintered density was achieved.

Figures 3 and 4 show SEM micrographs of samples sintered at 1300°C for 15 minutes using 20 K min^{-1} and 250 K min^{-1} heating rates respectively. The sintered densities are 57% and 76% of the theoretical density respectively which reflects the much reduced level of porosity in Fig. 4.

Agglomeration effects on density

Figure 5 is a medium magnification SEM micrograph of sample 9, sintered to the highest density of 92%. Even at this density large 100 μm pores remain. It is likely that these large pores derive from agglomeration of the starting alloy powders during size reduction milling. Figure 6 is an SEM micrograph of the $Fe_2Al_5/FeAl_2$ powder, illustrating an agglomerate of around 50 μm in diameter. Upon reaching additive melt temperature a 50 μm pore would be formed.

Table 1 Sample experimental parameters and results

Sample	Heating rate, K min^{-1}	Sintering temperature, °C	Green density, %	Sintering time, min	Sintered density, % of theoretical	Densification, %
1	20	1300	73	0	66·3	−24·8
2	20	1300	73	15	65·4	−28·0
3	150	1300	60	0	64·25	10·6
4	400	1300	60	15	80·25	50·6
5	150	1350	60	0	64·93	12·3
6	400	1350	60	15	84·75	61·8
7	150*	1300	55	0	73·75	41·6
8	400*	1300	55	15	88·64	74·7
9	150*	1350	55	0	74·79	44·0
10	400*	1350	55	15	84·45	65·4

*Using 5·67 μm $Fe_2Al_5/FeAl_2$ particles

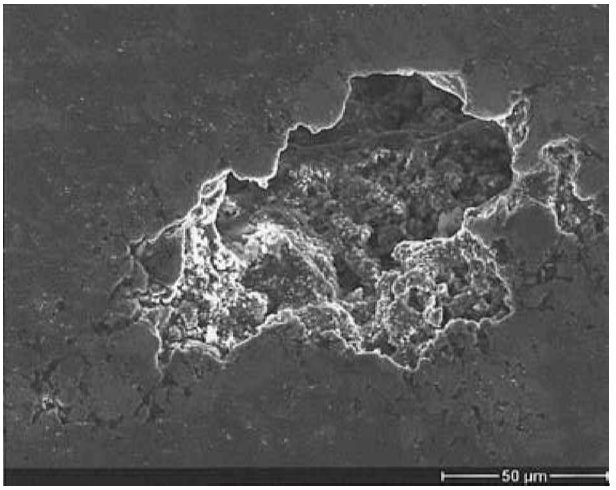

5 SEM micrograph of 92% dense sample, revealing large isolated pores surrounded by dense matrix

Capillary behaviour dictates that a liquid phase is drawn into the interparticle pores to a depth that is dependent upon contact angle, liquid viscosity, pore size as described in equation (2)

$$x^2 = \frac{d_p \gamma_{LV} t \cos\theta}{4\eta} \quad \ldots\ldots\ldots\ldots (2)$$

where x is liquid penetration depth (μm), d_p is pore size, γ_{LV} is liquid vapour surface energy (j), t is time (s), θ is contact angle, η is liquid viscosity (Pa s^{-1}).

Once the 50 μm agglomerate melts, the liquid is drawn deeper into the smaller surrounding pores, leaving a large pore behind, which would require a great degree of solid sintering to remove.

Time

For specimens heated at 150 K min^{-1}, 250 K min^{-1} and 400 K min^{-1} and then held at 1300°C or 1350°C for 15 minutes, there is a density increase (Fig. 7). The initial densification of the specimens, particularly those with fine 6 μm particle sizes, was extensive. Densities of 80–85% were observed where no holding time was employed. Such rapid initial densification suggests that the particle rearrangement stage is active in the early stages of sintering, indicating liquid presence after the additive melting point is passed. Continued sintering time increased density further, with a maximum achieved after 15 minutes in all cases using the 150 K min^{-1}, 250 K min^{-1} or 400 K min^{-1} heating rate.

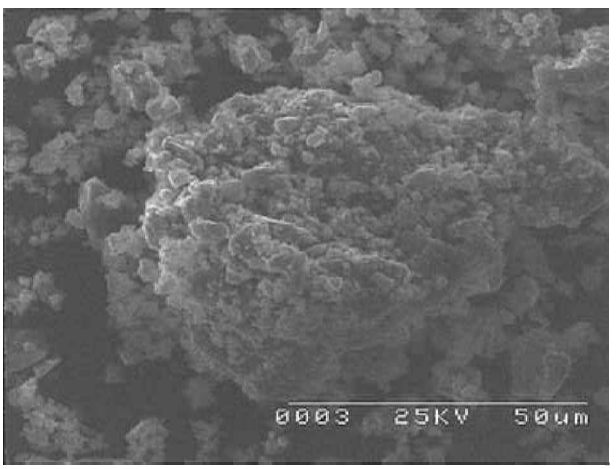

6 SEM micrograph of alloy powder agglomerate from 5·67 μm powders

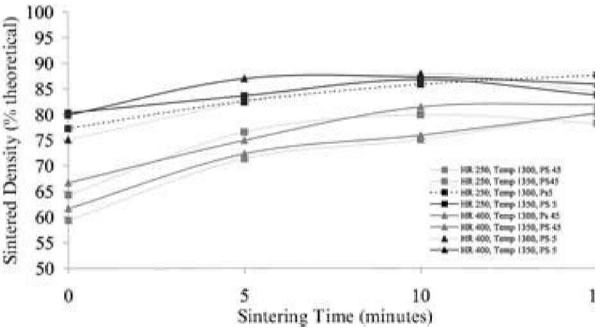

7 Comparison of density of sintered Fe_3Al using 250 and 400 K min^{-1} heating rates over periods of up to 15 min

Longer sintering times may produce even higher densities in samples heated with a 250 or 400 K min^{-1} heating rate, as the density values were not decreasing after 15 minutes. In some samples heated at 150 K min^{-1}, a density decrease for sintering times greater than 10 minutes was observed as discussed above. This is probably due to Ostwald ripening, suggesting that the optimum sintering time had been passed.

Sintering effects of $Fe_2Al_5/FeAl_2$ additive

Liquid phase sintering theory indicates that once the additive liquefies, rapid rearrangement of the solid particles is possible if sufficient liquid is present. Rearrangement can induce rapid densification if conditions are right. After rearrangement, the chemical potential gradient across the solid Fe/liquid $Fe_2Al_5/FeAl_2$ interface, will result in diffusion of aluminium from liquid to solid. Once sufficient aluminium has diffused across the liquid/solid interface, compact solidification will occur. Solid state sintering mechanisms now govern the continued sintering and densification of the inhomogeneous solid compact (neglecting minor viscous flow contributions from an intermediate supersolidus liquid). The solidification of the liquid, as opposed to total dissolution into the solid (observed with elemental transient liquids), could be instrumental in the prevention of Kirkendall porosity at additive particle sites.

Figure 8 shows the iron–aluminium equilibrium diagram.[21] The likelihood of swelling is indicated by the solubility ratio, which is a division of the solubility of the liquid in solid S_{ls} by the solubility of solid in liquid S_{sl} (equation (3)).

$$\frac{S_{ls}}{S_{sl}} = S_R \quad \ldots\ldots\ldots\ldots (3)$$

In the case of elemental iron and aluminium the solubility ratio is 0·0004. Where $Fe_2Al_5/FeAl_2$ is used, the solubility ratio

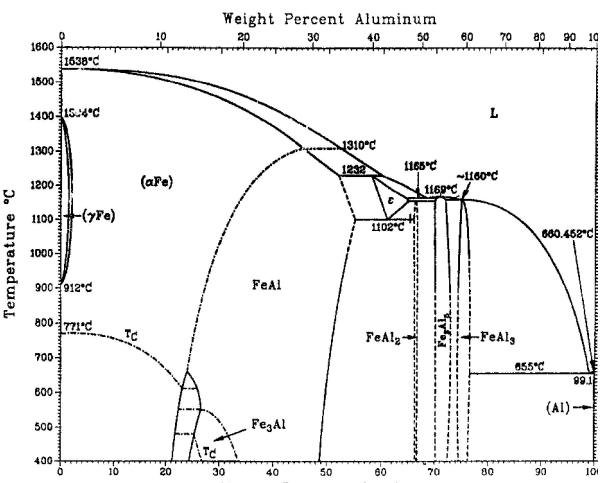

8 Fe–Al equilibrium phase diagram

(estimated from the phase diagram) is around 0·1. After liquid formation the solubility ratio rises to around 0·27 (also estimated from the phase diagram) at 1300°C, which is favourable for effective sintering between these powders at higher temperatures.

The mismatched diffusion and solubility rates that cause Kirkendall porosity are significantly reduced by production of Fe_3Al under these conditions.

CONCLUSIONS

1. High density iron–aluminide (Fe_3Al) compacts were produced as a result of transient liquid phase sintering, using rapid heating techniques and a mixture of prealloyed $Fe_2Al_5/FeAl_2$ and elemental Fe powders.
2. A 20 K min^{-1} heating rate did not allow a transient liquid to form and consequently compact densification did not occur. The 150, 250 and 400 K min^{-1} heating rates did cause densification.
3. The density of green compacts increased with increasing sintering time, to a maximum after 15 minutes.
4. The properties of the prealloyed powder additive are favourable for transient liquid phase sintering which accounts for the greater part of the density increase.
5. A green compact, produced from powder of constitution 50% iron and 50% $Fe_2Al_5/FeAl_2$ and with a mean particle size of 5·67 μm, gave a sintered density of 92% using a 250 K min^{-1} heating rate.

ACKNOWLEDGEMENTS

This work was performed as a part of a PhD programme supported by GKN.

REFERENCES

1. M. JOHNSON, D. E. MIKKOLA, P. A. MARCH and R. N. WRIGHT: *Wear*, 1990, **140**, (2), 279–289.
2. S. C. DEEVI and V. K. SIKKA: *Intermetallics*, 1996, **4**, 357–375.
3. S. C. DEEVI, V. K. SIKKA and C. T. LIU: *Prog. Mater. Sci.*, **42**, (1/2), 177–192.
4. C. G. MCKAMEY, J. A. HORTON and C. T. LIU: *Scr. Metall. Mater.*, 1988, **22,** 1679.
5. A. AGARWAL and R. BALASUBRAHAMIAN: *Bull. Mater. Sci.*, 1996, **19**, (1), 91–102.
6. A. BAHADUR, B. R. KUMAR and O. N. MOHANTY: *J. Mater. Sci.*, 1995, **30**, (14), 3690–3696.
7. C. CLARK, R. N. WRIGHT, J. K. WRIGHT and B. H. RABIN: *Scr. Mater. Metall.*, 1995, **32**, (11), 1883–1888.
8. L. ANTHONY and B. FULTZ: *Acta Metall. Mater.*, 1995, **43**, (10), 3885–3891.
9. N. K. XYDAS: 'Pressureless sintering of high density tri-iron aluminide', PhD thesis, South Bank University, London, UK, 2001.
10. R. M. GERMAN: 'Liquid phase sintering'; 1985, London, Plenum Press.
11. S. K. SAVITSKII and N. N. BURTSUV: *Sov. Powder Metall. Met. Ceram.*, 1981, **20**, 618.
12. S. K. SAVITSKII, N. N. BURTSUV and L. S. MARTUNSOVA: *Sov. Powder Metall. Met. Ceram.*, 1982, **21**, 760.
13. A. BOSE, B. RABIN and R. M. GERMAN: *Powder Metall. Int.*, 1988, **20**, (3) 25–30.
14. A. BOSE, R. A. PAGE, W. MISIOLEK and R. M. GERMAN: 'Advances in powder metallurgy', Vol. 6, 135–145; Princeton, NJ, MPIF.
15. X. Q. WANG, G. FAIR and J. V. WOOD: *Powder Metall.*, 1993, **36**, (3), 187–191.
16. X. Q. WANG and J. V. WOOD: *Powder Metall.*, 1995, **38**, (1), 59–65.
17. W. H. BAEK and R. M. GERMAN: *Int. J. Powder Metall.*, **22**, (4), 235–245.
18. W. H. BAEK and R. M. GERMAN: *Powder Metall. Int.*, 1985, **1**, (6), 205–213.
19. R. M. GERMAN and J. W. DUNLAP: *Metall. Trans. A*, 1986, **17A**, 205–213.
20. W. H. BAEK and R. M. GERMAN: *Powder Metall. Int.*, 1985, **17**, (6), 273–279.
21. D. J. LEE and R. M. GERMAN: *Int. J. Powder Metall. Powder Technol.*, **21**, (1), 9–21.